Development 138, 1195-1205 (2011) doi:10.1242/dev.057570

Apical ectodermal ridge morphogenesis in limb development is controlled by *Arid3b*-mediated regulation of cell movements

Jesus C. Casanova, Veronica Uribe, Claudio Badia-Careaga, Giovanna Giovinazzo, Miguel Torres and Juan Jose Sanz-Ezquerro*

SUMMARY

The apical ectodermal ridge (AER) is a specialized epithelium located at the distal edge of the limb bud that directs outgrowth along the proximodistal axis. Although the molecular basis for its function is well known, the cellular mechanisms that lead to its maturation are not fully understood. Here, we show that *Arid3b*, a member of the ARID family of transcriptional regulators, is expressed in the AER in mouse and chick embryos, and that interference with its activity leads to aberrant AER development, in which normal structure is not achieved. This happens without alterations in cell numbers or gene expression in main signalling pathways. Cells that are defective in *Arid3b* show an abnormal distribution of the actin cytoskeleton and decreased motility in vitro. Moreover, movements of pre-AER cells and their contribution to the AER were defective in vivo in embryos with reduced Arid3b function. Our results show that *Arid3b* is involved in the regulation of cell motility and rearrangements that lead to AER maturation.

KEY WORDS: Limb development, *Arid3b*, AER, Morphogenesis, Organogenesis, ARID, Mouse, Chick

INTRODUCTION

Vertebrate limb development is a classic model in embryology for the study of pattern formation and morphogenesis (Duboc and Logan, 2009; Tickle, 2003; Zeller et al., 2009). Limbs arise from the lateral plate mesoderm as small buds composed of undifferentiated mesenchyme covered by ectoderm, and interactions between these tissues are crucial for the induction, outgrowth and patterning of the limb. Several important signalling centres that regulate these processes are established in the limb bud. Among them, the apical ectodermal ridge (AER) directs outgrowth along the proximodistal axis. The AER is a thickened, specialized epithelium that is located at the tip of the bud at the dorsoventral border (Fernandez-Teran and Ros, 2008). In its mature form, it is a columnar pseudostratified epithelium in chick and a polystratified epithelium in mammals, covered by a peridermal layer. It expresses several signalling molecules from different pathways, particularly members of the Fgf family, which mediate its function. The AER is a transient embryonic structure that shows very dynamic morphological and gene expression changes during its activity.

Initially, and as consequence of Fgf10 signalling from the lateral plate mesoderm that is mediated by Wnt signals, cells in the pre-bud ectoderm start expressing Fgf8. These cells are considered to be the precursors of the AER and in this early phase they cover a wider area of ectoderm, both in dorsal and ventral regions in chick but showing a ventral restriction in mouse embryos. Moreover, early Fgf8 expression is patchy, indicating a mixing of expressing and non-expressing cells. This domain is referred to as pre-AER. It is only later that Fgf8-expressing cells associate at the dorsoventral (DV) boundary to give rise to a more compact structure that will evolve into the mature AER with its characteristic histological appearance. However, the processes governing this compaction are not fully understood. It has been proposed that movements of cells are crucial to achieve the normal stratification and AER morphology, but the contribution of active migration, cell intercalation, differential adhesion or cell sorting to this process is not clear (Tickle and Altabef, 1999).

The ARID family of transcriptional regulators is an evolutionary conserved group of genes that perform essential functions in eukaryotic organisms from yeast to humans (Wilsker et al., 2002). It is characterized by a distinctive DNA-binding domain (the AT-rich interacting domain, ARID), which is highly conserved among its members. Proteins of this family have been implicated in regulation of cell cycle, gene expression and differentiation, and have important roles in embryonic development. They seem to function as context-dependent transcriptional regulators that can act as activators or repressors, and also show chromatin-remodelling activities.

A founder member of this family is the *Drosophila* gene *dead ringer* [*dri*, also known as *retained* (*retn*)] (Shandala et al., 2002). *dri* is essential for *Drosophila* development and is involved in several aspects of embryonic patterning and differentiation (Shandala et al., 1999; Shandala et al., 2003), including wing development (Shandala et al., 2002). Vertebrate orthologues of *dri* comprise three genes that form the Arid3 group. The best characterised is *Arid3a/Bright/Dril1*, which is involved in regulating immunoglobulin heavy chain expression in B-lymphocytes (Herrscher et al., 1995). An oncogenic potential of *Arid3a* has also been proposed (Peeper et al., 2002). With respect to *Arid3c*, no information about its expression or functions is available so far.

Department of Cardiovascular Developmental Biology, Centro Nacional de Investigaciones Cardiovasculares, CNIC, Melchor Fernández Almagro, 3, Madrid 28029, Spain.

*Author for correspondence (jjsanz@cnic.es)

Accepted 23 December 2010

Arid3b/BDP/Dril2 is the third factor of the subfamily. It was first cloned in a two-hybrid screening as a protein that binds to retinoblastoma protein (Numata et al., 1999) and it has been implicated in tumourogenesis, specifically in the development of malignant neuroblastoma (Kobayashi et al., 2006). *Arid3b* has been shown to be sufficient to immortalize mouse embryo fibroblasts (MEFs) in vitro and to confer malignancy to MEFs in vivo when co-expressed with MycN. Moreover, *Arid3b* is expressed in human neuroblastoma cell lines and in stage IV tumours (but not in stage I-III), indicating a possible role in the progression of malignant neuroblastoma. Interestingly, other data indicated an essential role for *Arid3b* during embryonic development (Takebe et al., 2006). Deletion of *Arid3b* in mouse led to embryo lethality around E11-E12, with severe craniofacial and cardiovascular malformations. However, the specific roles of this gene are not completely understood.

Here, we show that *Arid3b* is expressed in the AER of mouse and chick embryos, and that its function is essential for a correct maturation of this important signalling centre. Moreover, *Arid3b*-deficient cells have reduced motility in vitro. Our results suggest that it controls a cellular program involved in cell rearrangements that are essential for organogenesis in the embryo.

MATERIALS AND METHODS

Embryos

Fertilised chick eggs (Rhode Island Red) were obtained from Granja Santa Isabel (Cordoba, Spain). Eggs were incubated at 38°C and chick embryos staged according to Hamburger and Hamilton (Hamburger and Hamilton, 1951). Mouse embryos were collected at the indicated gestational stage (E0.5 was defined as noon of the day on which a vaginal plug was detected). Embryos were fixed in 4% PFA (overnight at 4°C).

Mouse gene-trap model and *Arid3b* mutant embryos

Heterozygous mice were generated from a Baygenomics ES cell line (RRJ028) with a genetrap in the *Arid3b* locus. *gt/gt* embryos were obtained by mating heterozygous animals. Embryos were genotyped by comparing β-Gal staining levels. Adult animals were genotyped by PCR.

Cloning of chick *Arid3b*

A PCR fragment was amplified from stage HH20-22 chick cDNA with *Arid3b* flanking primers designed from Ensembl browser sequence information. Mutations for dominant-negative versions of c*Arid3b* were introduced using the QuickChange Site-directed Mutagenesis kit. The GenBank Accession Number for the chicken *Arid3b* nucleotide sequence reported here is HQ830030.

In ovo electroporation

Limb fields of stage HH10-11 chick embryos were electroporated using a TSS20 electroporator (Intracel, Hertfordshire, UK) fitted with 0.3 mm width custom-made platinum electrodes. The plasmid DNA or morpholino solution was poured over the ectoderm of the right prospective limb and five pulses at 10 V were applied. Embryos were re-incubated at 38°C and collected at different times. Left limbs were used as controls.

Morpholino oligonucleotides

Morpholinos were purchased from Gene Tools (Philomath, OR, USA). The *cArid3b*-specific morpholino corresponds to the exon3-intron3 junction and was conjugated with lissamine. A control morpholino (fluorescein conjugated) supplied by the manufacturer was used.

Bead implantation

Recombinant FGF10 or FGF8 (1 mg/ml; R&D systems, Minneapolis, MN, USA) was loaded on heparin-acrylic beads and the inhibitor SU5402 (2 mg/ml; Calbiochem, Gibbstown, NJ, USA) was loaded on AG1-X2 beads for 1 hour. Beads were implanted into stage HH19-20 limb bud mesenchyme beneath the AER or into stage HH15 lateral plate mesoderm.

RNA in situ hybridization on whole-mount and paraffin wax sections

Non-radioactive (digoxigenin) whole-mount hybridization was performed according to standard protocols based on those of Nieto et al. (Nieto et al., 1996) for chick embryos and of Wilkinson and Nieto (Wilkinson and Nieto, 1993) for mouse embryos. In situ hybridisation on sections (7 μm) was carried out from PFA-fixed and paraffin wax-embedded embryos.

Immunohistochemistry

Cell markers were detected by immunohistochemistry on 8 μm cryostat or 5 μm paraffin sections, using standard protocols for fixation, inclusion and sectioning.

Proliferation and cell death

Cell death was detected using a TUNEL kit (Roche, Basel, Switzerland). Cell proliferation was assessed by BrdU incorporation or phospho-Histone3 labelling. Samples were mounted in Vectashield containing DAPI (1.5 μg/ml). The total numbers of nuclei and BrdU-positive, PH3-positive and TUNEL-positive cells were counted in sections from three embryos per condition.

Alcian Green staining

Embryos fixed in 5% TCA were stained for cartilage with Alcian Green.

MEF culture, staining and migration

Mouse embryonic fibroblasts were obtained from E9.5 embryos. Embryos were placed in a 100 μm pore grid (BD-Falcon) and disaggregated with a 1 ml syringe plunger. The cell suspension was plated on 24-well tissue culture plates with culture medium [DMEM enriched with glucose and glutamine (Sigma), 15% FBS and 1% penicillin/ampicillin]. Cells were fixed in 4% PFA for phalloidin staining.

To monitor migration, cells were cultured in six-well culture plates and videos were recorded over a minimum of 3 hours, beginning at least 8 hours after seeding. Recordings were made with a Nikon Eclipse Ti microscope equipped with a cell culture chamber and time-lapse recording software. Cell movements during selected 3-hour windows were tracked with MetaMorph software.

DiI labelling of chick embryos

Chick embryos (HH10-11) were electroporated with the DN-*Arid3b* or control plasmids, and 12 hours post-electroporation (HH14-15) cells were labelled with DiI with a capillar glass needle within the electroporated area, in a region between 200 and 400 μm lateral to the medial part of the somites, caudal to somite 15 (this area corresponds to pre-AER cells (see Altabef et al., 1997). Embryos were collected 36 hours post-electroporation (HH19-20) and the contribution of labelled cells to the AER was recorded.

RESULTS

Arid3b is expressed in the AER in mouse and chick embryos

In the course of a candidate gene screen looking for new genes potentially involved in vertebrate limb development, we decided to analyse the expression pattern of vertebrate orthologues of *Drosophila dead ringer*. The expression of *Arid3b* was analysed by in situ hybridisation in both chick and mouse embryos at different stages of development. Among other embryonic structures (including branchial arches, somites, neural tube and notochord) we saw a clear expression in the apical ectodermal ridge of limb buds, both in whole mount (Fig. 1A-C) and in sections (Fig. 1D,E). Expression of *Arid3b* was first observed in the pre-limb bud ectoderm from stage 16-17 in chick (Fig. 1F) and from E9.5 in mouse (Fig. 1G), in both cases preceding *Fgf8* expression but appearing later than other early ridge markers such as *Sp8* (see Fig. S1A,B,E,F in the supplementary material). Initially, *Arid3b* is expressed in dorsal and ventral ectoderm, but later on high levels of expression are present only in the apical ectodermal ridge

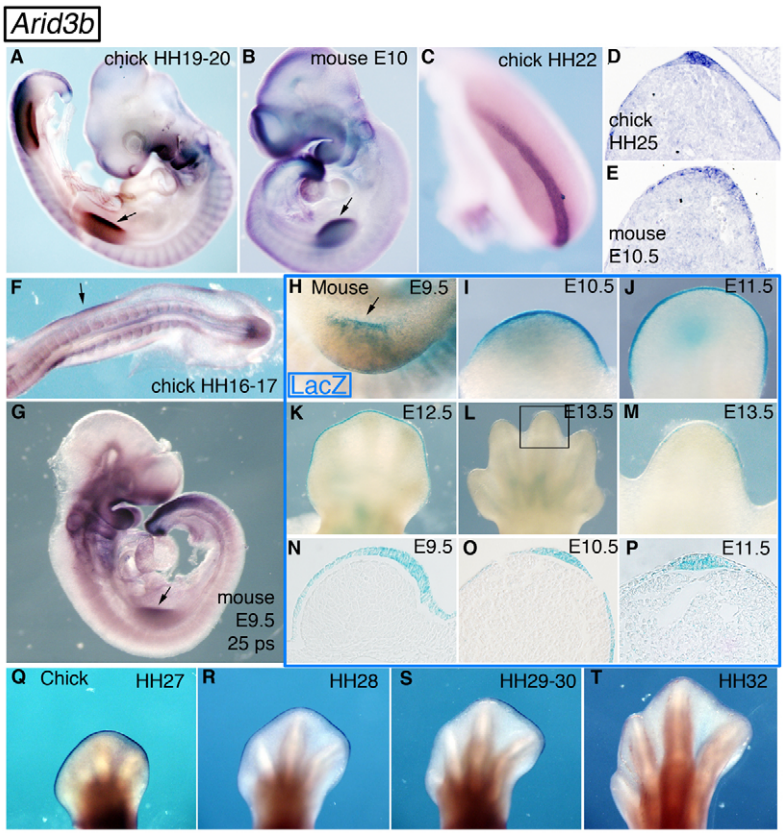

Fig. 1. *Arid3b* is expressed in the AER of chick and mouse embryos. Stages correspond to Hamburger and Hamilton (HH) for chick embryos and days of gestation [embryonic day (E)] for mouse embryos. (**A-G**,**Q-T**) RNA in situ hybridization showing expression of *Arid3b* in whole-mount specimens (A-C,F,G) or paraffin wax-embedded sections (D,E). Expression of *Arid3b* is detected in the AER, from early stages up to the end of digit patterning. (**H-P**) β-Gal staining in whole-mounts and sections of limbs from heterozygous embryos. Expression is detected in the limb ectoderm at E9.5 (H,N) and in the AER up to E13.5-E14 in the tip of digits (L; M is a magnification of boxed digit 3 in L). Arrows point to pre-AER (F,G) or AER (A,B,H).

(Fig. 1D,E,N-P; see Fig. S1B in the supplementary material). Expression in the AER persisted up to stage 30 in the chick (Fig. 1Q-T) or to E13.5 in mouse (Fig. 1H-M).

To confirm that *Arid3b* expression is associated with AER development, we induced ectopic AERs by overexpression of a constitutively active form of β-catenin. These indeed showed *Arid3b* expression (n=3; see Fig. S1D in the supplementary material). Additionally, we induced ectopic limbs by application of Fgf8-soaked beads to the flank of chick embryos. Twenty hours later, extra limb buds had been induced that showed *Arid3b* expression in the AER (see Fig. S1C, part a in the supplementary material). Moreover, *Arid3b* expression was regulated by Fgf signalling in limb buds: application of Fgf10 beads in the mesenchyme showed an anteriorly expanded *Arid3b* domain (see Fig. S1C, part b in the supplementary material); conversely, application of the FGFR inhibitor SU5402 produced a downregulation of *Arid3b* expression (see Fig. S1C, part c in the supplementary material). All these data demonstrate that *Arid3b* expression is associated with AER formation.

Arid3b is necessary for the correct maturation of the AER

To gain insight into the function of *Arid3b* in AER development, we performed gain- and loss-of-function experiments in the chick embryo. To achieve this, we first cloned the chick gene from HH20-22 whole embryo cDNA. The predicted sequence of 560 amino acids (see Fig. S7 in the supplementary material) showed a high degree of conservation with mouse and human orthologues, particularly in the ARID domain.

Functional experiments in chick embryos were carried out by electroporation of pre-limb bud ectoderm with *Arid3b*-expressing plasmids and a plasmid encoding GFP that was included to monitor the electroporated areas. Only ectoderm (and not mesenchyme) was targeted with high, albeit variable, efficiency and cells expressing GFP also expressed ectopic *Arid3b* at higher levels than the endogenous gene (see Fig. S2A,B in the supplementary material). Electroporation with the control plasmid did not cause an increase in cell death or alterations in AER formation, *Fgf8* expression or limb patterning (n=11, see Fig. S2B,C in the supplementary material).

Overexpression of wild-type chick *Arid3b*, on the contrary, lead to AER malformations, as evidenced by morphology and *Fgf8* expression 48 to 72 hours post-electroporation (Fig. 2; see Table S1 in the supplementary material). A high percentage of GFP-positive embryos (92% of cases at 48 hours, 100% at 72 hours) showed alterations in the AER. This included branched AERs with regions of *Fgf8* expression in the dorsal or ventral ectoderm (Fig. 2A,D), irregular morphologies and borders (Fig. 2B,E), or the presence of discontinuous AERs with areas lacking *Fgf8* expression (Fig. 2C,F). In the most extreme forms, almost a complete absence of AER was observed. Interestingly, wild-type chick *Arid3b* was not able to induce expression of *Fgf8* (Fig. 2B, arrows). Skeletal pattern was analysed in embryos collected at 5-9 days post-electroporation. In 56% of surviving embryos (n=36), alterations in the normal skeletal pattern were observed. In half of the affected limbs, ectopic skeletal elements (cartilage condensations and digits, Fig. 2G) or soft tissue overgrowths (Fig. 2H) were present. In the other half of cases, severe truncations in the proximodistal (PD) axis were observed (Fig. 2I). These data show that overexpression of wild-type *Arid3b* leads to abnormal AER development.

For loss-of-function experiments, two approaches were undertaken: overexpression of dominant-negative (DN) versions of *Arid3b* and electroporation of morpholino oligonucleotides. For

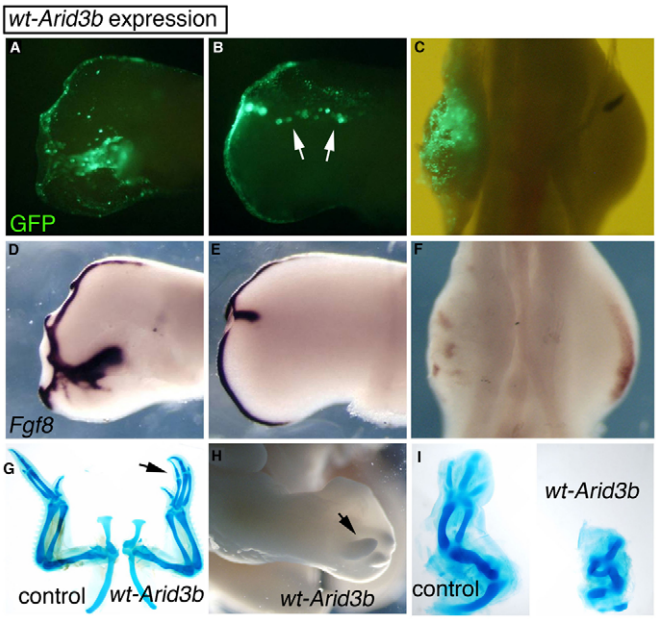

Fig. 2. Overexpression of wild-type *cArid3b* in chick ectoderm leads to AER malformations. (**A-C**) GFP fluorescence and (**D-F**) *Fgf8* expression in limbs 48 hours after co-electroporation with GFP and wild-type *cArid3b* expression plasmids. Panel pairs A and D, B and E, C and F show the same limbs. Defects range from ventral or dorsal stretches of AER (D), localised disruptions to the endogenous ridge (E), to large gaps in the AER lacking *Fgf8* expression (F). Arrows in B indicate GFP-positive regions not expressing *Fgf8*. (**G-I**) Skeletal defects in electroporated limbs collected 5-7 days post-electroporation include extra elements such as fingers (G, arrow), soft tissue outgrowths (H, arrow) and truncations (I). (A-F) Ventral views; electroporated limbs on the left in C,F. (G-I) Dorsal views; electroporated limbs on the right in G,I. (A,B,D,E,H) Legs. (C,F,G,I) Wings.

DN overexpression, mutations were introduced in chick *Arid3b* precisely mimicking those that had been shown to act in a dominant-negative fashion in closely related members of the family both in vivo (drosophila *Dri*) (Shandala et al., 2002) and in vitro [mouse and human *Arid3a* (previously known as *Bright*) (Nixon et al., 2004; Rajaiya et al., 2006)]. These comprised a short helix deletion or a point mutation in the ARID domain (Fig. 3A). Plasmids were electroporated and embryos with high levels of GFP were collected at 24, 48 and 72 hours post-electroporation. Similar results were obtained with both constructs. Again, no defects were apparent at 24 hours (before AER had formed). However, in 55% of embryos collected at 48 hours (n=36/66) a malformed AER was observed. This consisted of the loss of a visible elevated AER in whole-mount specimens at the time of collection. When *Fgf8* expression was analysed by in situ hybridisation, an abnormal AER, shorter in the anteroposterior (AP) axis but wider in the dorsoventral (DV) axis, was seen [when compared with the control limb (Fig. 3B)]. Moreover, it had irregular borders and lacked a mature histological structure, as confirmed on sections (Fig. 3C,D). At 72 hours post-electroporation, the results were similar: in 57% of electroporated embryos (n=26/46) clear defects in AER compaction, as monitored by *Fgf8* expression, were observed both in whole mount and in sections. In the majority of those embryos (21 cases in total) AER alterations involved a flattened structure without stratification of cells. In 24% (n=5/21) of collected embryos at 5-9 days post-electroporation, skeletal defects were present, mainly the presence of ectopic elements, which included digits (Fig. 3E) combined with truncations.

As a complementary strategy, we knocked down the expression of *Arid3b* by using morpholino oligonucleotides directed to a splicing region in the pre-mRNA. Morpholinos were electroporated and embryos collected at 30 hours post-electroporation (Fig. 3F). An altered AER phenotype was observed in 47% of those embryos (n=7/15). *Fgf8* expression was shortened in the AP axis, widened in the DV axis and the AER was not compacted properly (Fig. 3G), a phenotype reminiscent of that obtained with the dominant-negative experiments. Electroporation of control morpholinos did not result in alteration of AER development or *Fgf8* expression (both appeared normal in 9/9 cases; see Fig. S2D in the supplementary material).

To further characterise the role of *Arid3b* and to analyse its possible requirement for mammalian AER formation, a mutant mouse was used (referred to as *Arid3b gt/gt*). This approach was based on a gene-trap line that had the *lacZ* gene inserted in the intron after the first coding exon of the gene, producing a predicted fusion protein lacking all the functional domains of *Arid3b*. Heterozygous animals were crossed to obtain embryos at midgestation times (E9.5-E10.5). As the exact insertion point of the vector could not be determined, the different expression levels of *lacZ* were used to unambiguously distinguish heterozygous from homozygous embryos by β-gal staining (see Fig. S3B in the supplementary material). First, we observed that the *lacZ* expression pattern in heterozygous embryos was similar to that previously observed by in situ hybridisation for *Arid3b*. Interestingly, we noted important malformations in homozygous embryos at E10.5, which led to early lethality. Although up to that stage the ratio of homozygous versus heterozygous embryos was as expected, from E10.5 the number of *Arid3b gt/gt* embryos was reduced and no surviving embryos were collected after E11.5 (see Fig. S3A in the supplementary material). Alterations at E10.5 comprised a general delay in growth and defects in various organs, especially severe craniofacial and cardiovascular malformations [as had been previously shown with another null model (Takebe et al., 2006)]. *Arid3b* function is thus necessary for correct embryonic development in mouse and its absence is lethal. Interestingly, there was also a limb defect in the *gt/gt* embryos that was previously not described. Owing to the delay in growth between *gt/gt* and wild-type embryos, we used a standardization method to accurately compare limbs at the same relative developmental stage (see Fig. S3C in the supplementary material). Limb buds from *gt/gt* animals were smaller than wild-type limbs and the morphology of the AER was altered, consisting of a wider AER with irregular DV borders, already apparent in the freshly collected specimens (Fig. 3H,I, arrow). When *Fgf8* expression was analysed by in situ hybridisation, an abnormal AER was observed, with a shorter AP length and a widened DV extension showing irregular borders (Fig. 3J,K). In limb sections analysed for *Fgf8* expression, a flat AER with only one or two cell layers was observed, thus lacking the polystratified structure of a normal AER at this age (Fig. 3L,M). However, in the few specimens that could be analysed at later time points (E10.5-11), AERs containing multiple layers, although with abnormal structure, could be seen (see later, e.g. Fig. S5C in the supplementary material).

All these results taken together show that *Arid3b* is not necessary for the expression of *Fgf8*. However, its function is essential for a correct compaction of *Fgf8*-expressing cells during maturation of the AER in chick and mouse embryos, which show very similar alterations upon loss of Arid3b function.

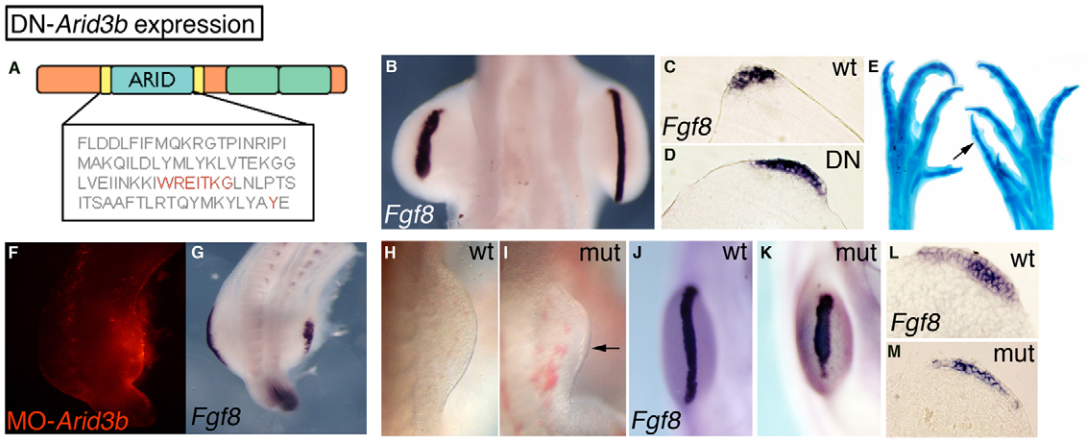

Fig. 3. Loss-of-function of *Arid3b* in chick and mouse embryos produces similar AER alterations. (**A**) Diagram showing in red the short helix deletion (amino acids 281-287) and the point mutation (Y312A) introduced in the ARID domain to yield two dominant-negative versions of *cArid3b*. (**B**) Ventral view of *Fgf8* whole-mount in situ hybridisation in a chick embryo electroporated (left limb) with *cArid3b*$^{DN\Delta hW}$ and collected 48 hours post-electroporation. The AER is shortened in the AP axis and widened in the DV axis compared with the control limb (right). (**C**,**D**) Paraffin wax-embedded sections of a chick embryo previously probed by in situ hybridisation for *Fgf8*. (C) Control limb showing typical pseudostratified AER. (D) Electroporated limb with flat morphology and dorsoventral extension of the AER. (**E**) Alcian Green stained limbs of a chick embryo collected 9 days post-electroporation with *cArid3b*$^{DN\Delta hW}$. Control limb on the left; electroporated limb on the right showing an anterior extra digit (arrow), which is also protruding ventrally. (**F**,**G**) Electroporation of chick limb bud with *cArid3b*-targeting morpholino oligonucleotides alters AER phenotype. (F) Embryo 30 hours post-electroporation showing the electroporated area (red fluorescence). (G) *Fgf8* in situ hybridisation of the same embryo. *Fgf8*-positive cells are non-compacted and the AER is shortened in the AP axis and widened in the DV axis, similar to the phenotype in B. (**H**,**I**) Right forelimbs from E10 wild-type (H) and E10.5 *gt/gt* (I) embryos; dorsal view. In the *gt/gt* limb, the AER has an altered morphology, widening and an irregular border (arrow). (**J**,**K**) Frontal views of E10.5 wild-type (J) and *gt/gt* (K) mouse forelimbs in situ hybridised for *Fgf8*. The phenotype is similar to the *Arid3b* loss-of-function in chick embryos. (**L**,**M**) Sections of wild-type (L) and *gt/gt* (M) limbs similar to those shown in J and K. Stratification is absent in *gt/gt* AER.

Mechanism of *Arid3b* function in AER morphogenesis

To determine the molecular mechanisms responsible for *Arid3b* effects in the AER, a series of markers involved in limb initiation and patterning were analysed in embryos with altered *Arid3b* function. First, the expression of genes important for AER induction such as *Fgf10* in the mesenchyme or *Sp8* and *Msx2* in the ectoderm was compared between wild-type and *gt/gt* embryos in mouse at E10.5. No alterations in the intensity or pattern of these genes could be seen (Fig. 4A). These results, together with the clear *Fgf8* expression observed in the loss-of-function contexts above, demonstrate that *Arid3b* is not required for the specification of pre-AER cells.

Second, markers for DV patterning, important for the correct positioning of the AER, were analysed both in *gt/gt* mouse embryos and in gain- and loss-of-function experiments in chick. Expression of *Wnt7a* (a dorsal ectoderm marker), *Lmx1b* (a dorsal mesenchyme marker), and *En1* and *Bmp7* (ventral ectoderm markers) was similar in wild-type and *gt/gt* embryos, all of them retaining their dorsal or ventrally restricted expression (Fig. 4B). Similarly, after electroporation of *DN-cArid3b* in chick and collection of embryos at 30 and 48 hrs post-electroporation, no differences in the expression of these markers could be seen, despite a clear alteration in the AER was already noticeable (Fig. 4D; see Fig. S4B in the supplementary material). Moreover, in chick embryos overexpressing wild-type *Arid3b*, no changes were observed in the expression of *Wnt7a*, *En1* or *Bmp7* (Fig. 4C; see Fig. S4A in the supplementary material). Interestingly, in embryos where abnormal AERs were detected, no ectopic DV borders were established (Fig. 4C). All these results strongly suggest that the effects produced by *Arid3b* are not related to the establishment of DV patterning.

Finally, expression of other genes of signalling pathways crucial for AER homeostasis was compared between wild-type and *gt/gt* mouse embryos at E10.5. These included *Dkk1*, a secreted inhibitor of the Wnt pathway, and *Serrate2*, a ligand of the Notch pathway. No differences in the expression pattern of these genes were detected (see Fig. S4C in the supplementary material).

The results presented so far suggest that *Arid3b* is not involved in the induction of the AER. To analyse whether cellular homeostasis was affected and could be responsible for the defects, cell proliferation and apoptosis were measured. Chick embryos were electroporated with the wild-type or *DN-cArid3b*-expressing constructs and collected at 30 hours post-electroporation (n=3 for each case). BrdU and TUNEL-positive cells were recorded in the AER of electroporated and contralateral limbs, and the percentages calculated and compared. In mouse embryos, similar analyses were performed at E10.5 comparing wild-type with *gt/gt* embryos (n=3, proliferation measured with PH3). Results are shown in Fig. 5 and in Table S2 in the supplementary material. Overexpression of wild-type *cArid3b* or *DN-cArid3b* did not lead to significant changes either in proliferation or apoptosis at 30 hours post-electroporation. In the case of mouse limbs, both proliferation and apoptosis were similarly reduced in *gt/gt* AERs at E10 (56% less PH3-positive cells and 64% less TUNEL-positive cells than control embryos). It is worth noting that in other tissues, proliferation was also reduced but apoptosis clearly increased in *gt/gt* embryos, as had been previously reported (Takebe et al., 2006). These results suggest that changes in cell number or an increase in apoptosis at the time of AER formation is not the cause of the observed defects in chick or mouse embryos that lack *Arid3b* function. Curiously, 72 hours after electroporation of *DN-cArid3b* in chick, proliferation levels were slightly

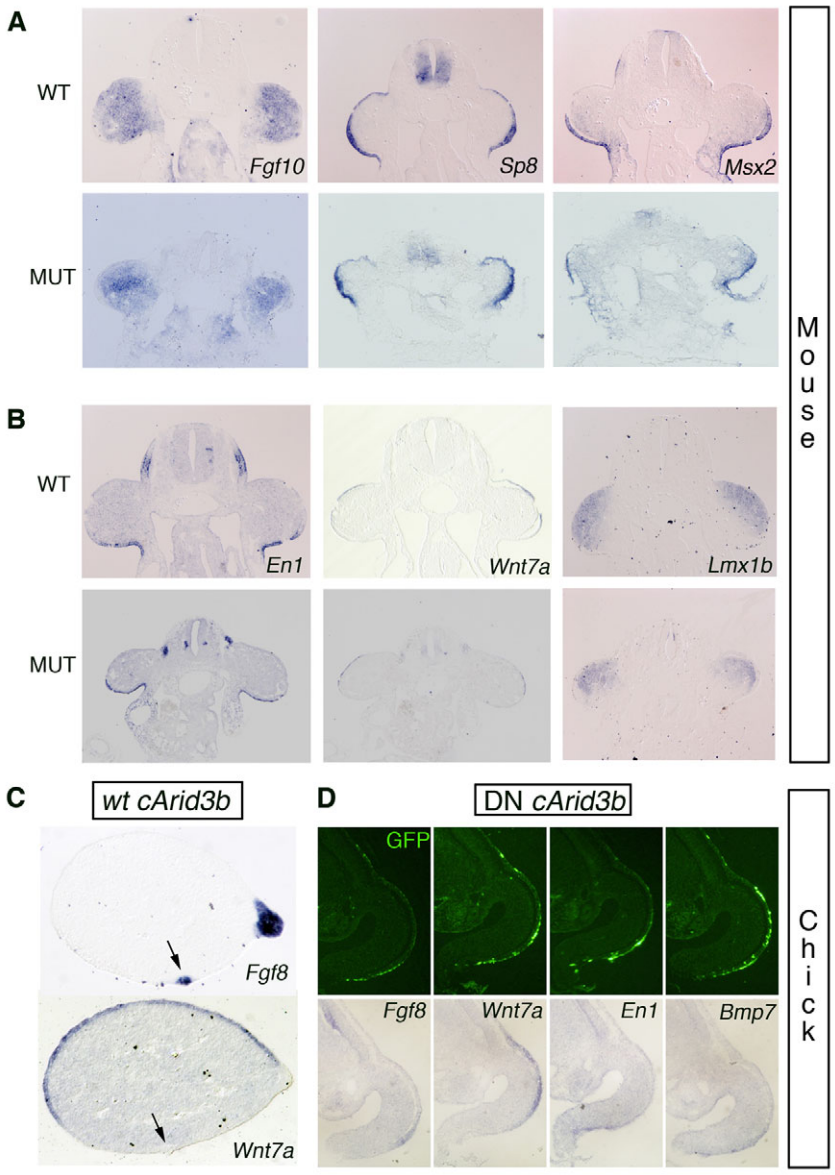

Fig. 4. *Arid3b* gain- or loss-of-function does not alter expression of markers of limb initiation or DV patterning. (**A**,**B**) In situ hybridisation for markers of limb bud induction (mesenchymal *Fgf10* and ectodermal *Sp8* and *Msx2*) and DV markers (ectodermal *En1* and *Wnt7a* and mesenchymal *Lmx1b*) on paraffin sections of E10 (wild type) and E10.5 (*gt/gt*) mouse limbs. Expression is similar in wild-type and *gt/gt* limbs. Representative images are shown of *n*=3 embryos for *Wnt7a* and *En1*, *n*=2 for all others. (**C**) *Fgf8* and *Wnt7a* expression in a chick limb overexpressing wild-type *cArid3b*. Embryo was collected at 72 hours post-electroporation and in situ hybridisation performed on transverse sections. An *Fgf8*-positive area of AER is present in the ventral ectoderm (arrows) without changes to *Wnt7a* expression. (**D**) Overexpression of *cArid3b*$^{DN\Delta hW}$ in chick ectoderm. Embryos were sectioned 30 hours post-electroporation. Analysis of ectodermal markers (bottom row) in electroporated areas (top row, GFP fluorescence in same sections) shows no alterations in expression patterns, despite overexpression of *DN-cArid3b* in dorsal and ventral ectoderm.

increased (although not statistically significant) and apoptosis was clearly reduced in electroporated AERs when compared with controls (Fig. 5B).

Our data thus suggested that *Arid3b* was involved in maturation of the AER and not in its initial specification. Further support for this came with the analysis of gap junction protein connexin 43 (Cx43). Cx43 is intensely expressed in AER cells as opposed to the rest of limb ectoderm and has been used as a distinctive marker for the ridge (Green et al., 1994; Yancey et al., 1992). When we analysed Cx43 expression, staining was observed specifically in the AER of both control chick and wild-type mouse limbs (Fig. 6), with a clear reinforcement at the base of the AER in chick. Expression of Cx43 in *DN-cArid3b* electroporated chick limbs (72 hours post-electroporation) was present at high levels in the distal region and not in the rest of the ectoderm. However, the staining labelled a flat layer of cells, lacking the compacted elevated structure of the normal AER (Fig. 6). Similarly, in *gt/gt* mouse limbs (E9.5-10), Cx43 expression was evident in the distal ectoderm, but lacking the multilayered structure of wild-type AER (Fig. 6). At later time points, Cx43 was still present in the disorganised AER that develops in mutant embryos (see Fig. S5E in the supplementary material). This result supports the idea that AER cells are being normally specified but that correct histological maturation is altered in the absence of *Arid3b* function.

To confirm these findings we analysed the distribution of additional markers of cellular morphology in loss of *Arid3b* function (*DN-cArid3b* overexpression in chick at 72-80 hours post-electroporation and *gt/gt* mouse at E10). Morphology of cells was visualised by phytohemaglutinin labelling of membranes and β-catenin, E-cadherin and β1-integrin immunodetection. Cytoskeletal structure was analysed by actin and tubulin labelling. Finally, detection of laminin in chick and fibronectin in mouse was used to observe the basal lamina and the extracellular matrix, respectively (see Fig. S5A,B in the supplementary material). In all cases, although their expression was present, their distribution and the organization of cells in AERs lacking *Arid3b* function was abnormal. In chick embryos, AERs from control limbs showed the characteristic appearance of a mature AER, with a pseudostratified structure and a basal confluence of cell membranes giving a fan-shape. However, AERs from *DN* electroporated limbs had an

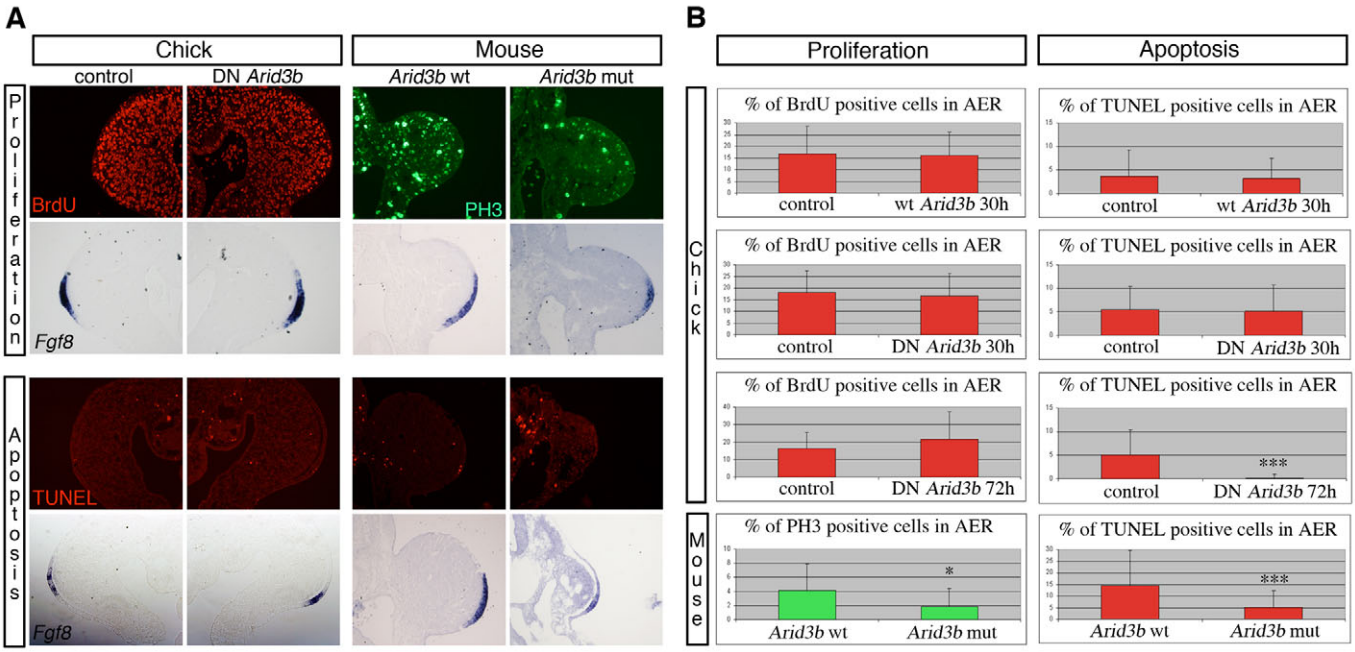

Fig. 5. Effect of *Arid3b* gain- and loss-of-function on proliferation and apoptosis in chick and mouse limbs. (**A**) (Left) Examples of contralateral (control) and *DN-cArid3b* electroporated chick limbs from embryos collected 30 hours post-electroporation. (Right) Wild-type E10 and *gt/gt* E10.5 mouse embryos. Proliferation was measured by immunohistochemistry with anti-BrdU (red) or anti-PH3 (green), and apoptosis was measured by TUNEL staining (red). Consecutive sections were in situ hybridised for *Fgf8* probe to identify the AER. (**B**) Quantitative analysis of proliferation and cell death. Data are the number of cells positive for each labelling as a percentage of the total number of *Fgf8*-positive cells in the AER (mean±s.d.; **P*<0.05, ****P*<0.01, Student's *t*-test).

aberrant, flat morphology, showing at most two or three layers of cells that lacked compaction. In wild-type mouse embryos, the AER was a polystratified epithelium. However, in *gt/gt* embryos, the AER consisted of a single layer of elongated cells (see, for example, E-cadherin, Fig. 6). At later stages (at 80 hrs post-electroporation in chick or E11 in mouse) the AER was hyperplastic, with multiple cell layers forming a disorganized mass that protruded towards the mesenchyme, lacking its normal histological appearance (see, for example, β-catenin in Fig. S5C in the supplementary material). Despite the abnormal structure, expression of *Fgf8* was still present (see Fig. S5B,C in the supplementary material). Moreover, protrusions towards the mesenchyme and a general irregular shape were seen, as opposed to the smooth contour of controls (e.g. laminin and fibronectin stainings; see Fig. S5A in the supplementary material). Sometimes, tubule-like structures were observed (see Fig. S5B,D in the supplementary material, arrows).

All these results show that morphogenesis of the AER is affected in the absence of *Arid3b* function. Although markers for cytoskeleton and cell adhesion are expressed, the maturation into a correct AER is compromised, involving both an initial delay in the process and a defective cell compaction later.

Arid3b is required for cell mobility of pre-AER cells

In chick electroporation experiments we observed that GFP-positive cells were uniformly distributed as individual cells in the ectoderm of control-electroporated embryos, whereas limbs expressing *DN-cArid3b* contained cell clusters (Fig. 7A). To investigate whether this was related to altered adhesion or migration, we analysed the cytoskeletal structure and in vitro migratory behaviour of *Arid3b*-deficient mouse embryonic fibroblasts (MEFs), which normally express *Arid3b* (see Fig. S6A in the supplementary material). MEFs from E9.5 *gt/gt* embryos had an abnormal general appearance, with fewer protrusions and a more compact shape than wild-type MEFs. Staining for actin revealed an increase in stress fibres and an aberrant distribution of actin filaments (Fig. 7B).

Migratory behaviour of MEFs was assessed by time-lapse video microscopy. MEFs from *Arid3b-gt/gt* embryos moved significantly slower and covered shorter distances than wild-type or heterozygous MEFs (Fig. 7C; see Movies 1 and 2 in the supplementary material). In the most extreme cases, *Arid3b-gt/gt* MEFs barely advanced, moving backwards and forwards; some cells indeed did not move at all. Cells sometimes emitted protrusions but these protrusions were significantly fewer in number (see Fig. S6B in the supplementary material) and looked abnormal (e.g. smaller than lamellipodia). Some cells that did move, left cell fragments behind, adhered to the plate. Many mutant MEFs also showed transient blebs protruding from the membrane (see Movie 2 in the supplementary material). By contrast, wild-type and heterozygous MEFs travelled extensively, often performing complex changes in direction and showed normal production of lamellipodia as they explored the environment (see Movie 1 in the supplementary material).

To test directly the role of *Arid3b* in AER cell mobility in vivo, cells in the pre-limb ectoderm of embryos that had been electroporated with *DN-cArid3b* or control plasmids were labelled with DiI and their contribution to the AER assessed 24 hours later (Fig. 8). Control electroporated DiI-labelled cells were present in the AER in all cases (*n*=5/5, Fig. 8D, arrow). However, DiI-labelled cells in *DN-Arid3b* electroporated embryos only

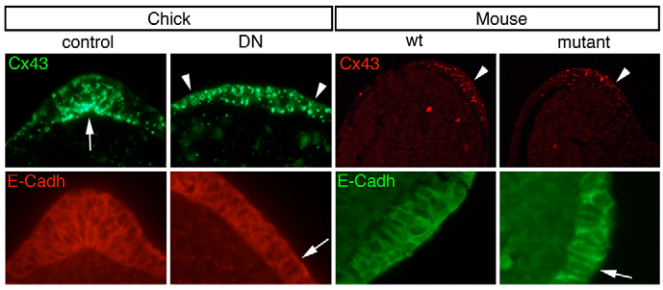

Fig. 6. *Arid3b* loss-of-function in chick and mouse limbs leads to defective AER morphogenesis. (Left) Chick embryos were electroporated with *DN-cArid3b* and collected 72-80 hours post-electroporation. (Right) E10 wild-type and E10.5 *gt/gt* mouse embryos. Sections at the level of AER were obtained and immunostained for Cx43 (top row) and E-Cadherin (bottom row). Top: Cx43 is expressed intensely in the control AER (arrow). However, although Cx43 is expressed in distal ectoderm only in *DN-cArid3b* electroporated limb, its distribution is broadened (arrowheads), lacking the compaction of control AER. In mouse, Cx43 is specifically expressed in the distal ectoderm, which nonetheless lacks the normal polystratification of wild type (arrowheads). Bottom: both chick and mouse AERs lacking *Arid3b* function show an abnormal structure when compared with controls. Elongated cells (arrows) are present and there is a lack of stratification.

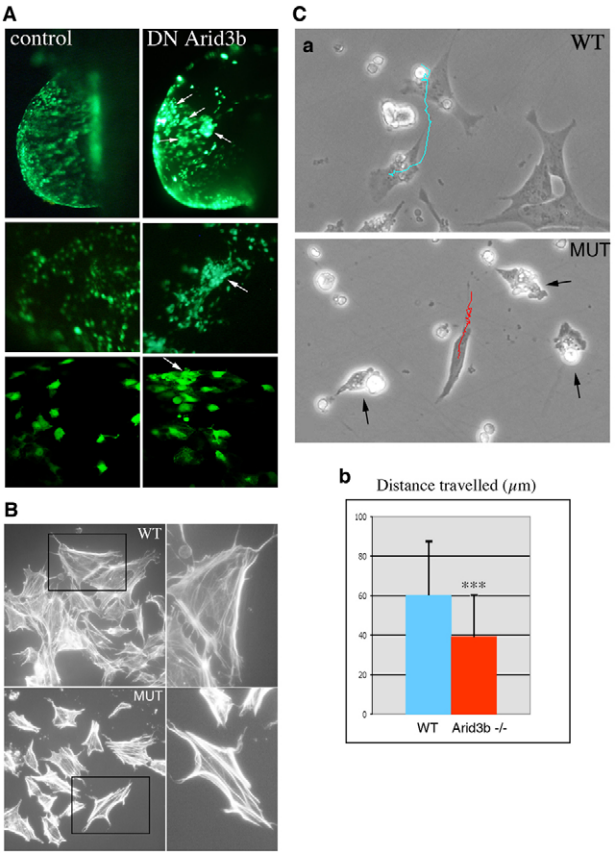

Fig. 7. *Arid3b*-deficient cells show abnormal actin cytoskeleton and defective migration in vitro. (**A**) Chick embryos were electroporated with control or *DN-cArid3b*-expressing plasmids and collected 48 hours post-electroporation. GFP fluorescence marks electroporated cells. Cells expressing *DN-cArid3b* tend to cluster (arrows), contrasting with the even distribution of cells electroporated with a control plasmid. (**B**) Phalloidin staining of the actin cytoskeleton of MEFs derived from E9.5 wild-type or *gt/gt* mouse embryos and cultured in vitro for 24 hours. Actin filaments in mutant cells are reduced in size, abnormally shaped and have aberrant distribution (selected cells are shown in the right-hand panels, rotated 90°). (**C**) Cell movements of in vitro cultured MEFs were filmed, and cell trajectories and travelled distances determined. (a) End time shots from a representative recording of cell movements; cell trajectories are superimposed in colour. Blebbing is present in mutant cells (arrows). (b) Quantification of travelled distance (mean±s.d. from 48 wild-type cells and 54 mutant cells. ***P<0.01; Student's t-test).

contributed to the AER in 15% of cases (n=2/13) and patches of DiI-labelled GFP-positive cells were observed in the ectoderm that were next to the AER, but did not reach it (Fig. 8H, arrow). This result strongly supports a function for *Arid3b* in regulating mobility of pre-AER cells.

DISCUSSION

Our results provide evidence of an important role for *Arid3b* in limb morphogenesis. The essential role of *Arid3b* in embryonic development (Takebe et al., 2006) has mostly been related to its effects on craniofacial and cardiovascular systems, but its role in the limb had not been appreciated. Our data show that *Arid3b* regulates limb development by controlling the correct maturation of one of its major signalling centres, the AER.

AER maturation is a poorly understood process. Despite being expressed at early phases of limb bud initiation, *Arid3b* is not necessary for the development of the AER in molecular terms. *Fg8* expression is induced normally in the absence of *Arid3b* function in both chick and mouse embryos and is maintained at normal levels even at advanced stages. This contrasts with the function of genes such as *Sp8*, which is not necessary for initial induction but is required to maintain *Fgf8* expression (Bell et al., 2003). Moreover, *Sp8* expression appears normal in the absence of *Arid3b*, suggesting that the regulatory relationship between the homologues of these genes in the early *Drosophila* embryo (where *dri* acts as a *buttonhead* repressor) (Shandala et al., 1999) is not conserved in the vertebrate AER. Gain-of-function experiments in chick show that *Arid3b* is not sufficient to induce *Fgf8* expression. This contrasts with the induction of ectopic *Fgf8* expression by activation of Wnt/β-catenin signalling (Kengaku et al., 1998) and suggests that *Arid3b* does not mediate this pathway.

In the chick electroporation experiments (both gain and loss-of-function), there was no strict correlation between the type or severity of the phenotype and the extent or position of the GFP-positive area. This suggests an origin for the AER alterations in cell-autonomous effects in target cells and possible non-autonomous effects on neighbouring cells, e.g. by overactivation of signalling pathways controlled by *Arid3b*. Alternatively, the phenotypes might originate in an exclusively cell-autonomous defect: an alteration in cellular motility (either increase or reduction) would disrupt proper AER morphogenesis whether target cells were AER precursors or nearby non-AER cells, as cell rearrangements would be affected in both cases.

The first noticeable alteration in loss-of-function studies was the persistence of a single layer of elongated cells, which is typical of the initial phases of AER formation but normally develops into the stratified epithelium of the mature AER. However, at later stages, limb buds lacking *Arid3b* contained many disorganised cell layers of *Fgf8*-expressing cells. This suggests that the initial steps of transformation of ectodermal

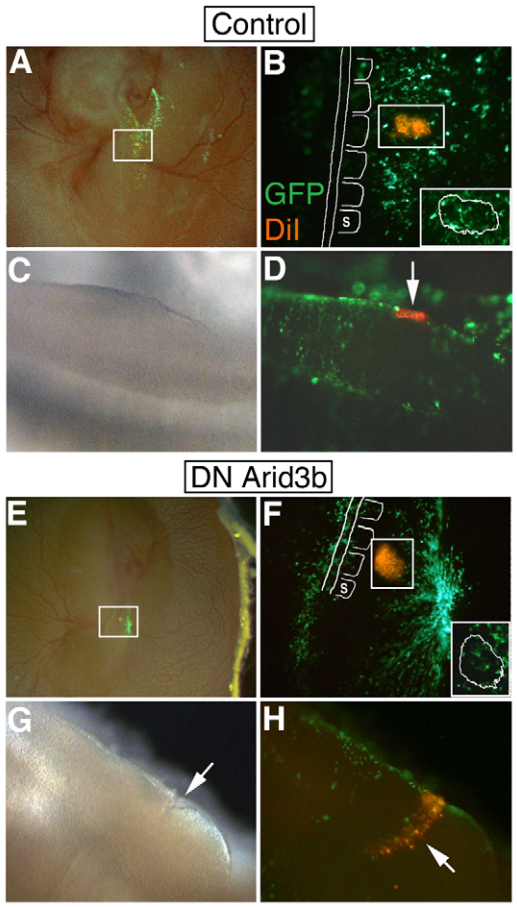

Fig. 8. *Arid3b*-deficient cells show defective contribution to the AER in vivo. (**A-D**) Control and (**E-H**) *DN-Arid3b* electroporated embryos were labelled with DiI 12 hours post-electroporation and the contribution of labelled cells to the AER was observed 36 hours later. (A,E) Embryos at the time of DiI injection (orange spots). Boxed areas are shown in detail in B,F, which are overlay images of green fluorescence marking electroporated cells and red fluorescence (that appears orange) marking DiI labelling. A spatial reference to somites is provided (s). Insets show the labelled area prior to DiI injection to appreciate the extent of electroporation. (C,G) Bright-field and (D,H) overlay of fluorescent images of experimental limbs 24 hours after DiI labelling. Morphology of the AER is altered in G (arrow) when compared with the control in C. Control DiI-labelled cells are located in the AER (D, arrow), whereas *DN-Arid3b*-electroporated DiI-labelled cells do not reach the AER (H, arrow).

cells into AER cells take place, but that the normal process of compaction is disrupted. This is also supported by the early expression of AER-specific markers, such as Cx43, in cells that subsequently fail to organize properly.

AER formation is sensitive to alterations to several signalling and patterning pathways. For example, activation of the Wnt pathway causes ectopic *Fgf8* expression whereas Wnt loss-of-function blocks AER formation (Barrow et al., 2003; Soshnikova et al., 2003). However, absence of *Arid3b* function did not affect *Fgf8* expression and the mesenchyme-ectoderm positive-feedback loop seems to operate as *Fgf10* expression was also normal. Other factors involved in AER induction, such as BMP signalling and its downstream target *Msx2* were also apparently unaltered. Similarly, expression of DV markers was unaffected by *Arid3b* manipulation, suggesting that this gene does not affect DV patterning. This contrasts with the abnormal DV patterning of the AER induced by BMP or En1 gain- or loss-of-function. Finally, elimination of *Notch1* or of the Notch ligand *jagged2/serrate2* from the limb has also been shown to disrupt AER development. However, *serrate2* expression is normal in *Arid3b gt/gt* embryos; and the skeletal phenotypes in the absence of *Arid3b* are different from those of Notch mutations, which mainly produce syndactyly. Thus, *Arid3b* loss-of-function defects appear not to be due to altered Notch signalling.

An interesting observation of our study is that, despite surprisingly *Fgf8* expression is maintained in abnormal AERs, skeletal defects are nevertheless produced. This suggests that, contrary to general statements (reviewed by Fernandez-Teran and Ros, 2008) AER morphology, rather than simply expression of signalling molecules, is crucial for proper AER function and correct limb development. It would be interesting to confirm whether the same skeletal defects are present in mice using a conditional knockout approach.

Proliferation and apoptosis in the nascent AER was unaffected in *Arid3b* gain- and loss-of-function experiments in chick, suggesting that altered cell numbers in the AER does not primarily cause *Arid3b* effects. In some cases, prolonged expression of DN-c*Arid3b* was associated with a noticeable reduction in cell death. However, we interpret this as a consequence of the phenotype rather than its cause: failed AER maturation at early stages would lead later on to aberrant cellular homeostasis with decreased cell death, producing the observed hyperplasic AERs. In mouse embryos, we did observe an early reduction in proliferation and apoptosis, but that was similar in magnitude, strongly suggesting that the balance in the number of cells is not the cause of the defects in the mouse AER either.

Collectively, our data suggest that *Arid3b* does not act on the molecular pathways or regulation of cell number required for AER induction and maintenance, and instead point to an involvement of *Arid3b* in AER maturation. Little is known about the cellular mechanisms underlying the transition from the simple ectodermal layer covering the early bud into a (pseudo)stratified epithelium. Although the reorganization of cells is obviously needed, the relative contribution of cell intercalation, active migration or changes in the plane of cell division is unknown. Recently, several papers have addressed the importance of mesenchymal oriented cell movements and divisions for limb development and proximodistal elongation (Boehm et al., 2010; Gros et al., 2010; Wyngaarden et al., 2010). A similar scenario, not fully appreciated so far, could be happening in the limb ectoderm and *Arid3b* function could be related to these processes, regulating for instance directional cell movements, oriented cell intercalation or cell polarity.

Fate map analyses in chick show that *Fgf8* expressing pre-AER cells initially cover a broad DV territory (Altabef et al., 1997) in a salt-and-pepper pattern, only later accumulating at the DV border of the distal limb. Moreover, lineage-tracing experiments in mice have determined the existence of two lineage boundaries (one located at the dorsal limit of the pre-AER and the other at the DV interface) that are essential for proper AER compaction and morphogenesis (Kimmel et al., 2000). It has been proposed that, via a zipper mechanism, ventral cells are pulled towards the dorsal margin and that bidirectional pulling toward the middle border elevates the AER (Loomis et al., 1998). Our findings support a role for *Arid3b* in those cell movements and rearrangements necessary for AER morphogenesis.

The absence of *Arid3b* results in AERs that are shortened along the AP axis and broadened in the DV axis. This suggests that AER maturation involves intercalation of cells anteroposteriorly and a compaction dorsoventrally, resulting in AP elongation and a DV narrowing. This process is reminiscent of convergent extension movements that occur during gastrulation (Wallingford et al., 2002) and it is possible that the cellular and molecular mechanisms that direct these movements also operate in AER formation. For example, it would be interesting to analyse the possible contribution of the non-canonical Wnt/planar cell polarity pathway (Simons and Mlodzik, 2008) to AER development, although current results from mouse mutants do not provide evidence for such a role [for example, *vangl2*- (Kibar et al., 2001) or *dact1*- (Suriben et al., 2009) null mice do not show apparent limb alterations]. Interestingly, the phenotypes of *Arid3b gt/gt* cells in vitro, including increased levels of actin stress fibres, extensive membrane blebbing and breakage of cells upon detachment from substrate are reminiscent of the effects of elevated Rho/Rac signalling, suggesting that *Arid3b*-deficient cells might have alterations in this important regulator of cell movements (Heasman and Ridley, 2008).

It will also be interesting to study the molecular targets of *Arid3b*. Members of the ARID family often act as part of multiprotein complexes to elicit their functions, interacting with various co-factors that modulate their activities (Valentine et al., 1998). Some of the closest homologues of *Arid3b* in vertebrates (especially *Arid3a*) have been shown to act as chromatin remodelling factors. Thus, the regulation of gene expression by *Arid3b* is likely to be complex and requires further investigation. Our results suggest that *Arid3b* is involved in a general programme to regulate cellular morphology, cytoskeletal structure and cell motility that might be important in many embryological processes.

Acknowledgements

We thank M. A. Ros, M. A. Nieto, A. Joyner, U. Rüther and J. L. de la Pompa for probes, and A. Morales and J. Galcerán for plasmids. This work was supported by grants from the Spanish Ministerio de Ciencia e Innovacion (BMC2003-06100 and BFU2006-12859/BMC) to J.J.S.-E., who was the recipient of a Ramón y Cajal contract; J.C.C. and V.U. were recipients of a FPU fellowship from the Spanish Ministerio de Educación. The CNIC is supported by the Spanish Ministerio de Ciencia e Innovación and the Pro-CNIC foundation.

Competing interests statement

The authors declare no competing financial interests.

Supplementary material

Supplementary material for this article is available at
http://dev.biologists.org/lookup/suppl/doi:10.1242/dev.057570/-/DC1

References

Altabef, M., Clarke, J. D. and Tickle, C. (1997). Dorso-ventral ectodermal compartments and origin of apical ectodermal ridge in developing chick limb. *Development* **124**, 4547-4556.

Barrow, J. R., Thomas, K. R., Boussadia-Zahui, O., Moore, R., Kemler, R., Capecchi, M. R. and McMahon, A. P. (2003). Ectodermal Wnt3/beta-catenin signaling is required for the establishment and maintenance of the apical ectodermal ridge. *Genes Dev.* **17**, 394-409.

Bell, S. M., Schreiner, C. M., Waclaw, R. R., Campbell, K., Potter, S. S. and Scott, W. J. (2003). Sp8 is crucial for limb outgrowth and neuropore closure. *Proc. Natl. Acad. Sci. USA* **100**, 12195-12200.

Boehm, B., Westerberg, H., Lesnicar-Pucko, G., Raja, S., Rautschka, M., Cotterell, J., Swoger, J. and Sharpe, J. (2010). The role of spatially controlled cell proliferation in limb bud morphogenesis. *PLoS Biol.* **8**, e1000420.

Duboc, V. and Logan, M. P. (2009). Building limb morphology through integration of signalling modules. *Curr. Opin. Genet. Dev.* **19**, 497-503.

Fernandez-Teran, M. and Ros, M. A. (2008). The apical ectodermal ridge: morphological aspects and signaling pathways. *Int. J. Dev. Biol.* **52**, 857-871.

Green, C. R., Bowles, L., Crawley, A. and Tickle, C. (1994). Expression of the connexin43 gap junctional protein in tissues at the tip of the chick limb bud is related to the epithelial-mesenchymal interactions that mediate morphogenesis. *Dev. Biol.* **161**, 12-21.

Gros, J., Hu, J. K., Vinegoni, C., Feruglio, P. F., Weissleder, R. and Tabin, C. J. (2010). WNT5A/JNK and FGF/MAPK pathways regulate the cellular events shaping the vertebrate limb bud. *Curr. Biol.* **20**, 1993-2002.

Hamburger, H. and Hamilton, H. L. (1951). A series of normal stages in the development of the chick embryo. *J. Exp. Morphol.* **88**, 49-92.

Heasman, S. J. and Ridley, A. J. (2008). Mammalian Rho GTPases: new insights into their functions from in vivo studies. *Nat. Rev. Mol. Cell Biol.* **9**, 690-701.

Herrscher, R. F., Kaplan, M. H., Lelsz, D. L., Das, C., Scheuermann, R. and Tucker, P. W. (1995). The immunoglobulin heavy-chain matrix-associating regions are bound by Bright: a B cell-specific trans-activator that describes a new DNA-binding protein family. *Genes Dev.* **9**, 3067-3082.

Kengaku, M., Capdevila, J., Rodriguez-Esteban, C., De La Pena, J., Johnson, R. L., Belmonte, J. C. and Tabin, C. J. (1998). Distinct WNT pathways regulating AER formation and dorsoventral polarity in the chick limb bud. *Science* **280**, 1274-1277.

Kibar, Z., Vogan, K. J., Groulx, N., Justice, M. J., Underhill, D. A. and Gros, P. (2001). Ltap, a mammalian homolog of Drosophila Strabismus/Van Gogh, is altered in the mouse neural tube mutant Loop-tail. *Nat. Genet.* **28**, 251-255.

Kimmel, R. A., Turnbull, D. H., Blanquet, V., Wurst, W., Loomis, C. A. and Joyner, A. L. (2000). Two lineage boundaries coordinate vertebrate apical ectodermal ridge formation. *Genes Dev.* **14**, 1377-1389.

Kobayashi, K., Era, T., Takebe, A., Jakt, L. M. and Nishikawa, S. (2006). ARID3B induces malignant transformation of mouse embryonic fibroblasts and is strongly associated with malignant neuroblastoma. *Cancer Res.* **66**, 8331-8336.

Loomis, C. A., Kimmel, R. A., Tong, C. X., Michaud, J. and Joyner, A. L. (1998). Analysis of the genetic pathway leading to formation of ectopic apical ectodermal ridges in mouse Engrailed-1 mutant limbs. *Development* **125**, 1137-1148.

Nieto, A., Patel, K. and Wilkinson, D. G. (1996). In situ hybridisation analysis of chick embryos in whole mount and tissue sections. In *Methods in Cell Biology*, vol. 51, pp. 219-235. New York: Academic Press.

Nixon, J. C., Rajaiya, J. and Webb, C. F. (2004). Mutations in the DNA-binding domain of the transcription factor Bright act as dominant negative proteins and interfere with immunoglobulin transactivation. *J. Biol. Chem.* **279**, 52465-52472.

Numata, S., Claudio, P. P., Dean, C., Giordano, A. and Croce, C. M. (1999). Bdp, a new member of a family of DNA-binding proteins, associates with the retinoblastoma gene product. *Cancer Res.* **59**, 3741-3747.

Peeper, D. S., Shvarts, A., Brummelkamp, T., Douma, S., Koh, E. Y., Daley, G. Q. and Bernards, R. (2002). A functional screen identifies hDRIL1 as an oncogene that rescues RAS-induced senescence. *Nat. Cell Biol.* **4**, 148-153.

Rajaiya, J., Nixon, J. C., Ayers, N., Desgranges, Z. P., Roy, A. L. and Webb, C. F. (2006). Induction of immunoglobulin heavy-chain transcription through the transcription factor bright requires TFII-I. *Mol. Cell. Biol.* **26**, 4758-4768.

Shandala, T., Kortschak, R. D., Gregory, S. and Saint, R. (1999). The Drosophila dead ringer gene is required for early embryonic patterning through regulation of argos and buttonhead expression. *Development* **126**, 4341-4349.

Shandala, T., Kortschak, R. D. and Saint, R. (2002). The Drosophila retained/dead ringer gene and ARID gene family function during development. *Int. J. Dev. Biol.* **46**, 423-430.

Shandala, T., Takizawa, K. and Saint, R. (2003). The dead ringer/retained transcriptional regulatory gene is required for positioning of the longitudinal glia in the Drosophila embryonic CNS. *Development* **130**, 1505-1513.

Simons, M. and Mlodzik, M. (2008). Planar cell polarity signaling: from fly development to human disease. *Annu. Rev. Genet.* **42**, 517-540.

Soshnikova, N., Zechner, D., Huelsken, J., Mishina, Y., Behringer, R. R., Taketo, M. M., Crenshaw, E. B., 3rd and Birchmeier, W. (2003). Genetic interaction between Wnt/beta-catenin and BMP receptor signaling during formation of the AER and the dorsal-ventral axis in the limb. *Genes Dev.* **17**, 1963-1968.

Suriben, R., Kivimae, S., Fisher, D. A., Moon, R. T. and Cheyette, B. N. (2009). Posterior malformations in Dact1 mutant mice arise through misregulated Vangl2 at the primitive streak. *Nat. Genet.* **41**, 977-985.

Takebe, A., Era, T., Okada, M., Martin Jakt, L., Kuroda, Y. and Nishikawa, S. (2006). Microarray analysis of PDGFR alpha+ populations in ES cell differentiation culture identifies genes involved in differentiation of mesoderm and mesenchyme including ARID3b that is essential for development of embryonic mesenchymal cells. *Dev. Biol.* **293**, 25-37.

Tickle, C. (2003). Patterning systems-from one end of the limb to the other. *Dev. Cell* **4**, 449-458.

Tickle, C. and Altabef, M. (1999). Epithelial cell movements and interactions in limb, neural crest and vasculature. *Curr. Opin. Genet. Dev.* **9**, 455-460.

Valentine, S. A., Chen, G., Shandala, T., Fernandez, J., Mische, S., Saint, R. and Courey, A. J. (1998). Dorsal-mediated repression requires the formation of a multiprotein repression complex at the ventral silencer. *Mol. Cell. Biol.* **18**, 6584-6594.

Wallingford, J. B., Fraser, S. E. and Harland, R. M. (2002). Convergent extension: the molecular control of polarized cell movement during embryonic development. *Dev. Cell* **2**, 695-706.
Wilkinson, D. G. and Nieto, M. A. (1993). Detection of messenger RNA by in situ hybridization to tissue sections and whole mounts. *Methods Enzymol.* **225**, 361-373.
Wilsker, D., Patsialou, A., Dallas, P. B. and Moran, E. (2002). ARID proteins: a diverse family of DNA binding proteins implicated in the control of cell growth, differentiation, and development. *Cell Growth Differ.* **13**, 95-106.
Wyngaarden, L. A., Vogeli, K. M., Ciruna, B. G., Wells, M., Hadjantonakis, A. K. and Hopyan, S. (2010). Oriented cell motility and division underlie early limb bud morphogenesis. *Development* **137**, 2551-2558.
Yancey, S. B., Biswal, S. and Revel, J. P. (1992). Spatial and temporal patterns of distribution of the gap junction protein connexin43 during mouse gastrulation and organogenesis. *Development* **114**, 203-212.
Zeller, R., Lopez-Rios, J. and Zuniga, A. (2009). Vertebrate limb bud development: moving towards integrative analysis of organogenesis. *Nat. Rev. Genet.* **10**, 845-858.

Table S1. Gain-of-function assays in chicken embryos

A Electroporation of wild-type Arid3b and collection of embryos at 48 hours (total electroporated embryos=37)

Alterations in AER morphology: 92% (*n*=34/37) (a)*		No apparent phenotype: 8% (*n*=3/37)
AER with abnormal shape: 74% (*n*=25/34)	Partial abscence of AER: 26% (*n*=9/34) (e)	
With branched AER: 40% (*n*=10/25) (b) One case with ectopic patch of Fgf8 expression away from endogenous AER (c)	AER not branched: 60% (*n*=15/25) (d)	

B Electroporation of wild-type Arid3b and collection of embryos at 72 hours (total electroporated embryos=15)

Alterations in AER morphology: 100% (*n*=15/15) (f)		No apparent phenotype: 0% (*n*=0/15)
AER with abnormal shape: 87% (*n*=13/15)	Partial abscence of AER: 13% (*n*=2/15) (j)	
With branched AER: 77% (*n*=9/13) (f,g) One case with ectopic patch of Fgf8 expression away from endogenous AER (h)	AER not branched: 23% (*n*=4/13) (i)	

*Letters in parentheses refer to images below, examples of each case.

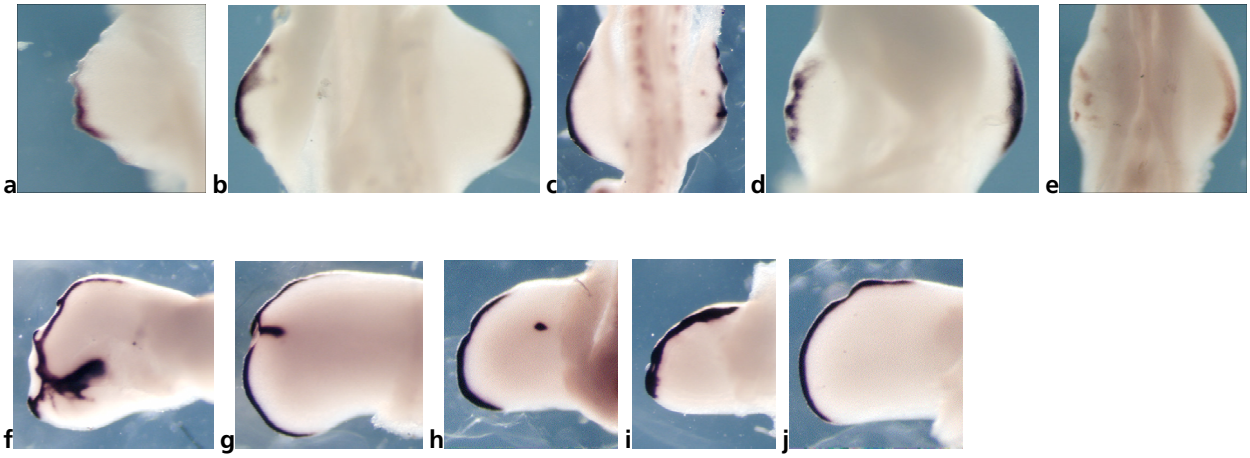

Table S2A. Complete data of proliferation/apoptosis in electroporated chicken embryos

		Arid3b wild type 30 hours control	Arid3b wild type 30 hours electroporated	Arid3b DN 30 hours control	Arid3b DN 30 hours electroporated	Arid3b DN 72 hours control	Arid3b DN 72 hours electroporated
Proliferation	Number of specimens	3	3	3	3	3	3
	Number of sections	22	27	29	29	25	9
	Number total Fgf8+ cells analysed	675	779	1093	1157	1011	448
	Number of Fgf8+ cells per section	30.68	28.85	37.69	39.90	40.44	49.77
	Number of total BrdU+ cells	112	125	200	193	166	96
	Percentage of BrdU+ cells per AER section average±s.d.	16.66±11.78	16.04±10.10	18.29±9.26	16.68±9.35	16.40±8.92	21.42±15.77
	Probability Student's *t*-test	0.36		0.40		0.26	
Apoptosis	Number of specimens	3	3	3	3	3	3
	Number of sections	15	16	27	30	18	18
	Number total Fgf8+ cells analysed	401	429	1109	1103	724	596
	Number of Fgf8+ cells per section	26.73	26.81	41.07	36.77	40.22	33.11
	Number of total TUNEL+ cells	15	14	61	57	36	1
	Percentage of TUNEL+ cells per AER section mean±s.d.	3.74±5.46	3.26±4.23	5.50±4.86	5.17±5.56	4.97±5.45	0.16±0.87
	Probability Student's *t*-test	0.30		0.29		0.0003***	

Table S2B. Complete data of proliferation/apoptosis in mouse embryos

		Arid3b wild type	Arid3b knockout
Proliferation	Number of specimens	3	3
	Number of sections	28	29
	Number total Fgf8+ cells analysed	1035	707
	Number of Fgf8+ cells per section	36.96	24.37
	Number of total BrdU+ cells	43	13
	Percentage of BrdU+ cells per AER section average±s.d.	4.15±3.8	1.84±3.01
	Probability Student's *t*-test	0.015*	
Apoptosis	Number of specimens	3	3
	Number of sections	55	25
	Number total Fgf8+ cells analysed	1999	673
	Number of Fgf8+ cells per section	36.35	26.92
	Number of total TUNEL+ cells	286	34
	Percentage of TUNEL+ cells per AER section average±s.d.	14.30±14.38	5.05±7.20
	Probability Student's *t*-test	0.001***	